Molecular Investigations of Selected Spike Protein Mutations in SARS-CoV-2: Delta and Omicron Variants and Omicron Subvariants

Urmi Roy[*]

[*]Department of Chemistry & Biomolecular Science

Clarkson University

8 Clarkson Avenue, Potsdam, NY 13699-5820, United States

[*]To whom correspondence should be addressed. E-mail: urmi@clarkson.edu;
ORCID iD: https://orcid.org/0000-0003-0928-0574

Abstract:

Among the multiple SARS-CoV-2 variants recently reported, the Delta variant has generated most perilous and widespread effects. Another variant, Omicron, has been identified specifically for its high transmissibility. Omicron contains numerous spike (S) protein mutations and in numbers much larger than those of its predecessor variants. In this report we discuss some essential structural aspects and time-based structure changes of a selected set of spike protein mutations within the Delta and Omicron variants. The expected impact of multiple-point mutations within the spike protein's receptor-binding domain (RBD) and S1 of these variants are examined. Additionally, the more recently emerged subvariants BA.4, BA.5 and BA.2.12.1 are discussed. Within the latter group, BA.5 represents globally, the most prevalent form of SARS-CoV-2 at the present time. Time-based mutations for the subvariant BA.2.75 are briefly explored. It is expected that the structural data discussed in this report will be helpful to identify drug targets and to neutralize antibodies for the evolving variants/subvariants of SARS-CoV-2.

Keywords: SARS-CoV-2; spike protein; structural biochemistry; Omicron subvariants; virus structure

1. Introduction

Since WHO declared a Public Health Emergency due to SARS-Cov-2 in January 2020 [1], several different variants of coronavirus have emerged. Among these variants, the Delta strain has been reported to be particularly aggressive due to its fast transmissibility and strong infectivity. The Delta variant, also known as the B.1.617.2 strain, was first identified in India, and was listed among the CDC's "Variants of Concern" [2]. The highly contagious B.1.1.529 strain, Omicron, was first identified in South Africa in December 2021 [3], and the presence of numerous spike (S) protein mutations in Omicron makes this variant highly transmissible. The BA.2 subvariant of Omicron, containing many additional mutations in its S protein has been a predominant COVID 19 species for several months until recently [4]. At this present time, another subvariant BA.5 largely represents the most active form of coronavirus worldwide. Among the other recent Omicron subvariants, BA.4 and BA.2.12.1 are also notable [5,6]. The mutations within the recent SARS-COV-2 variants and subvariants are listed in Supplementary Materials (SM) Table S1 and SII. As new variants/sub variants of SARS-CoV-2 continue to emerge, they are likely to be associated with more epitope escape mutations with epidemiological fitness.

High performance computational tools have the potential of aiding the ongoing efforts to identify the proper therapeutic targets for these pathogenic variants. In this regard, structure-based computational immunology and bioinformatics based methods of immuno-engineering play a critical role in detecting proper drug targets as well as in designing new vaccines [7-9].

In previous reports, the author has discussed the time-based structures of various immunologically significant proteins and their structure-functions relationships [10-12]. We have also reported the impacts of mutations on the receptor binding domain (RBD) of SARS-CoV-2

[13,14]. Recently we have also examined the impact of Zn ion coordinated Angiotensin II peptides on the spike 1 (S1)-angiotensin converting enzyme-2 (ACE2) receptor binding [15]. In the present communication, we will analyze most of the RBD mutations observed in the Delta and Omicron variants and Omicron subvariants BA.2, BA.4/BA.5 and BA2.12.1 and also determine their structural changes and stability as functions of time. Results for the time based structures of wild type (wt) SARS-CoV-2 S1 and the S1 mutations within the Delta, Omicron, and BA.2 will also be included here. A Recent report indicates that the Omicron subvariant BA.2 has multiple point mutations similar to those of Omicron variant and several Omicron subvariants, including BA.2 belong to Omicron [2]. However, previously identified BA.2 may contain several different mutations. Since the BA.2 variant described in this report is based on that earlier data, and since SARS-CoV-2 mutations tend to be variable, the data based on older version of BA.2 was not removed. The formerly identified BA.2 subvariant is labelled as BA.2 throughout this report [2]. Subvariants BA.4 and BA.5 contain identical RBD mutations, the details of which are included in tables S 1 and S 2 [16].

Recently a few cases of Deltacron recombinant species are identified in some countries. However, the phylogenetic tree of SARS-CoV-2 Omicron subvariants BA.1, BA.1.1, BA.2, BA.2.12.1 and BA.4/5 do not reflect proximity between the Delta and Omicron variants [17]. The RBD and S1 mutations within the Mu variant are also briefly explored here as well. The Mu was briefly discussed in this report was described as “Variants Being Monitored” by CDC [2]. Another relatively new subvariant BA.2.75, are also included in the SM section [16].

2. Materials and Methods

2.1. Mutation Steps

The spike (S) protein of the SARS CoV-2 comprises two subunits, S1 and S2. This paper is centered on the wt and recent mutant variants of the RBD and S1 subunit. The X-ray crystal structure 6M0J.PDB was selected for the wt RBD simulations [18]. Starting from the wt RBD structure, the mutant variants were generated using the VMD mutator plugin graphical user window (GUI). Since most of the mutations are within the newly emerged subvariants, and since these types of mutations tend to evolve consistently, they are frequently created in the computational approach. We have analyzed the selected RBD mutations within the B.1.617.2 strain, the Delta variant and the B.1.1.529 strain, the Omicron variant, along with an exploration of the subvariants BA.2, BA.4/BA5 and BA.2.12.1.

The I-TASSER server was used to model the structure of SARS-CoV-2 S1 [19]. The wt S1 was mostly prepared based on the CryoEM structure of 6VYB.PDB; chain B [20]. Due to the lack of experimental data, part of the protein sequences have still been missing in the published literature, making those sequences difficult to model; some of these missing sequences have been based here on the PDB structure 6ZP2 and other resources reported elsewhere [4,21]. In addition to the RBD mutations, wt, Delta, Omicron and BA.2 have been also examined in terms of their S1 characteristics.

The current work is a continuation of our previously published report [14], where the RBD mutations within B.1.1.7, B.1.351, and P1 lineages were discussed; these mutations were initially found in the UK, South Africa, and Brazil. The S1 sub unit of Delta strain based on 6Z97.PDB was also briefly mentioned there [14]. This present communication, discusses the RBD of Omicron and its newly emerged subvariants. In addition, a comparison of the Delta and Omicron S1 is carried out using a larger model structure where most of the missing sequences are restored.

The B.1.621 strain, also known as the mu variant and subvariant BA.2.75, are briefly mentioned in the SM. Initially, the BA.4/BA.5 subvariant were considered to have two mutations L452R, F486V and a reversion of Q493R [5]. To examine the implications of this consideration, the RBD of a possible subvariant with two mutations L452R and F486V alongwith the reversion of Q493R are also discussed in the SM section. These results help to establish a perspective for comparing the earlier description with the latest version of BA.4/BA.5. The current version of the BA.4/BA.5 contains mutations that exist in the newer form of BA.2 in addition to the above two mutations and a reversed mutation. The selected RBD and S1 mutations used in all simulation experiments have been listed in Table S1 and S2, and some of the mutations have been updated further through the course of this study.

2.2. MD Simulations

For the simulation purpose the QwikMD and NAMD packages were used. For the data analyses and visualization VMDprogram was utilized [22-24]. The implicit solvation system was used with the Generalized Born Solvent-Accessible Surface Area [16]. Initially the PSF structure files were prepared by deleting atoms and renaming residues. Energy minimization was performed for 2000 steps, and annealing was executed for 0.24 ns using a temperature increase from 60K to 300K. Equilibration was performed for 0.04 ns at 300K. After performing the initial minimization, annealing and equilibration steps, the MD production run was procured using the NVT ensemble. In all cases the integration time was selected for 2fs. The CHARMM36 force field was applied for all simulations.

For the annealing and equilibration protocols, the backbone atoms were restrained, while no atoms were constrained during the final MD simulation. The detailed experimental

procedures have been described elsewhere [13]. The exploratory simulations described in this report are based on the initial conformational samplings that provide a general insight into the proteins' predominant structural details. The resulting data were analyzed using VMD and the figures for reporting were developed using Biovia Discovery Studio Visualizer [25]. The plots of processed data were generated using origin.

3. Results and Discussions

The RBD of 6M0J.PDB contains residues 333 to 526. The RBD mutations on 6M0J are displayed in Fig.1 A-E. Fig. 1A includes the 3 mutations within the Delta/ B.1.617.2 strain selected for this study. Fig. 1B includes the 15 selected mutations within the Omicron/B.1.1.529 strain. Fig. 1C displays the 18 selected mutations within the Omicron BA.2 subvariant. Fig.1D and 1E represents the RBD mutations within the subvariants BA.4 or BA.5 and BA.2.12.1. Fig.1F-H depicts the S1 mutations in Delta, Omicron variants and Omicron subvariant BA.2.

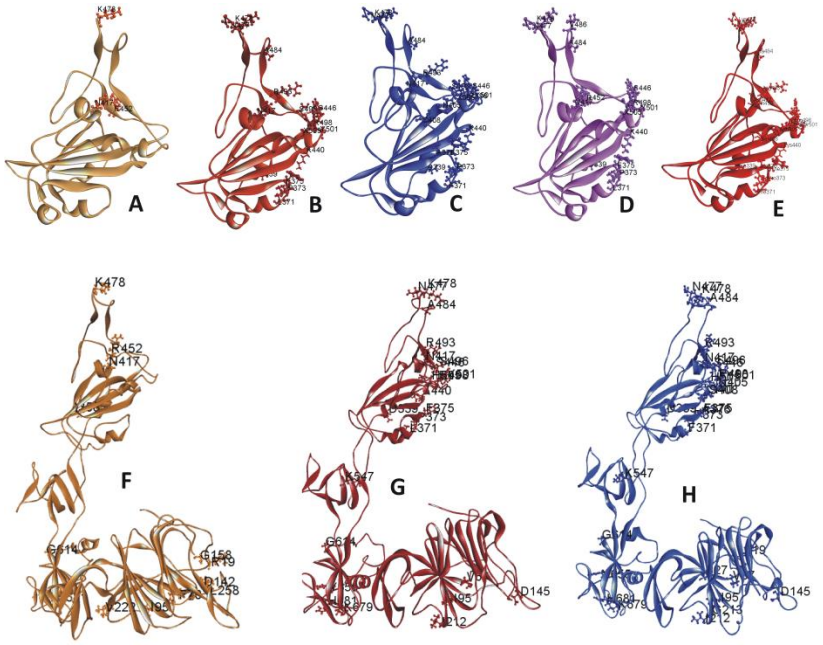

Figure 1. A-E Ribbon diagram of SARS-CoV-2 variants and subvariants with selected RBD mutations. These variants are based on 6M0J structure. Displayed are the RBD of A. Delta variant B. Omicron

variant C. Omicron BA.2 subvariant. D. Omicron BA.4/BA.5 subvariant and E. Omicron BA.2.12.1 subvariant with selected RBD mutations F-H. Ribbon diagram of SARS-CoV-2 variants and subvariant with selected S1 mutations. The mutant variants and subvariant structures are based on model S1. Displayed are the S1 of F. Delta variant G. Omicron variant and the H. subvariant BA.2 with selected S1 mutations.

Table S1 and S2 list the descriptive features of these mutations. The mutations within mu variant, subvariant BA.2.75, along with a potential subvariant with two mutations are also tabulated there. The RBD mutations of other variants have been described in our previous report [14].

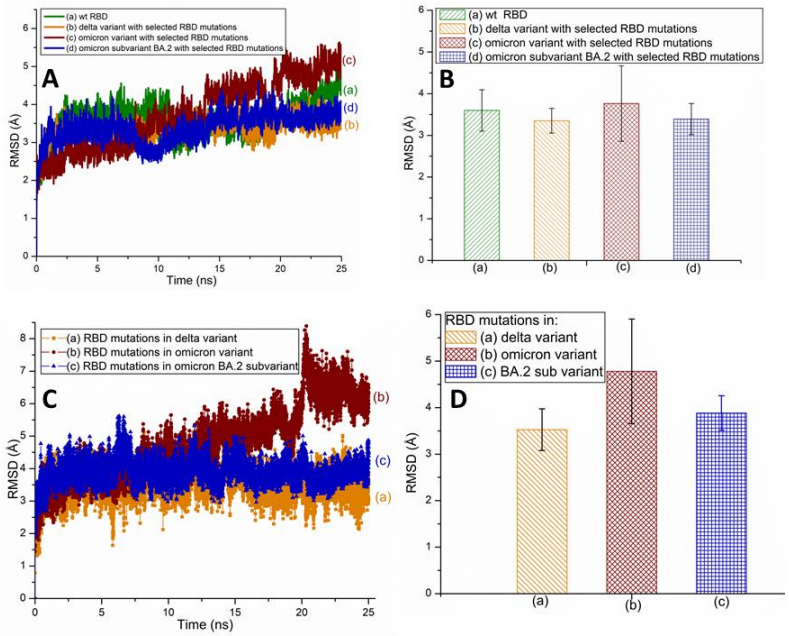

Figure 2. A. The typical all atom RMSD plots of wt and different SARS-CoV-2 variants and subvariant with selected RBD mutations. These variants and subvariant are based on 6M0J structure. B The average RMSD values of wt RBD, Delta, Omicron and BA.2 subvariant with selected RBD mutations. These values are extracted from Fig. 2A. The average RMSD value was taken from a 25ns simulation time. C. The typical RMSD plots of RBD mutations within different SARS-CoV-2 variants and subvariant. D. The average RMSD values of SARS-CoV-2 mutations within deferent variants and subvariant. These values are extracted from Fig. 2C. In all cases the all atom RMSD values are considered.

Fig. 2A illustrates the traditional all atom RMSD plots of wt and different SARS-CoV-2 variants and subvariant with selected RBD mutations; wt SARS-CoV-2 has also been included here for comparison. It is evident from these plots that Delta RBD is the most stable form among

all species studied here. This variant is more stable than Omicron and even stable compare to its wt version. While the Omicron variant is most unstable, the RBD of BA.2 is also quite stable. The average root mean square deviation (RMSD) of the BA.2 subvariant is slightly higher (3.4Å) than that of the Delta variant (3.35Å) as displayed in Fig. 2B. Fig. 2B also describes the average all atom RMSD results within the wt (3.6Å) and the Omicron (3.76 Å) species. The Delta variant has the lowest average RMSD value while Omicron has the highest. This figure also indicates certain findings from Fig. 2A, where the Omicron variant shows larger variations. Fig. 2C presents the RMSD plots of RBD mutations within different variants. The results in Figs 2C-2D suggest that the mutations within the Delta variant (3.52Å) are most stable and those of Omicron are most unstable (4.78Å). It is possible that numerous RBD mutations within the Omicron make the latter unstable; this is not the case for the RBD of Omicron subvariant BA.2, where the presence of RBD mutations make this protein rather stable (3.88Å). While the earlier version of the BA.2 has been examined in this work, the recently updated information from the CDC should be noted in this context, according to which, the BA.2 belongs to Omicron [2].

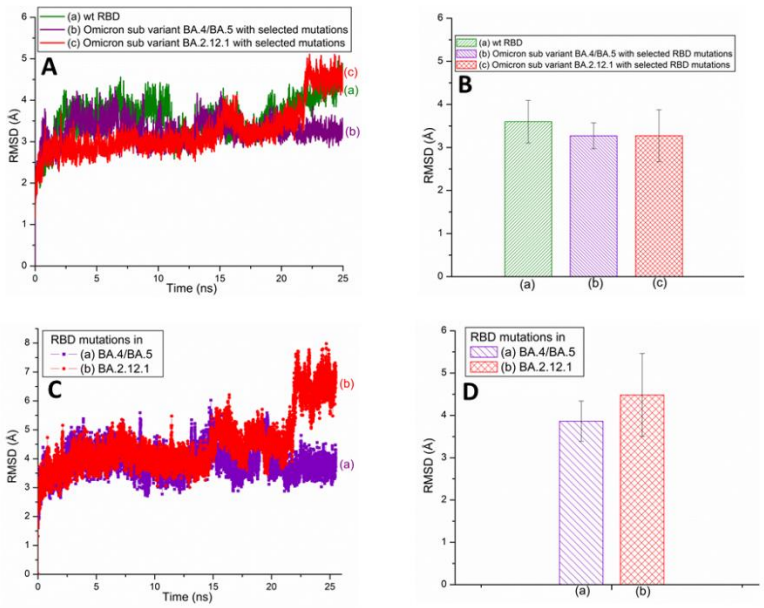

Figure 3. A. The typical all atom RMSD plots of wt and recently emerged SARS-CoV-2 Omicron subvariants with selected RBD mutations. These subvariants are based on 6M0J structure. B The average RMSD values of wt RBD, subvariants BA.4/BA.5 and BA.2.12.1 with selected RBD mutations. The values were taken from the 25 ns simulation time. These values were extracted from Fig. 3A. C. The typical all atom RMSD plots of RBD mutations within subvariants BA.4/BA.5 and BA.2.12.1. D. The average RMSD values for SARS-CoV-2 mutations within deferent subvariants. The average values were extracted from Fig. 3C.

Fig. 3A illustrates traditional all atom RMSD plots of the SARS-CoV-2 Omicron subvariants, BA.4/BA.5 and BA.2.12.1 with selected RBD mutations. The average RMSD values of these subvariants are displayed in Fig. 3B. From Fig.3A-B it is evident that RBD RMSD of subvariant BA.4/BA.5 (RMSD value: 3.26Å) is almost equal to that of BA.2.12.1 (RMSD value:3.27Å). However the RMSD values of the mutations observed within these two subvariants demonstrated that the BA.4/BA.5 mutations have a lower RMSD value of 3.86Å compare to 4.48Å of BA2.12.1. Accordingly, the mutations within BA.4/BA.5 are more stable than those existing within BA.2.12.1. This also implies that the mutations within BA.4/BA.5 are unstable compare to its entire RBD (Figs. 3 and S1). The all atom RMSD of RBD mutations within these two subvariants are plotted in Fig. 3C-3D. Therefore, though the BA.4/BA.5 RBD is more stable than Delta RBD overall, the RBD mutations within Delta (RMSD value: 3.52Å) are more stable than those of BA.4/BA.5 (3.86Å) and Omicron (4.78Å) variants, as well as those of BA.2 (3.88Å) and BA.2.12.1 (4.48Å) subvariants (Figs 2C-D and 3C-D). The RMSD of a possible subvariant with two mutations L452R and F486V is plotted in SM Fig. S1. The RBD RMSD graphs of Mu variant and BA.2.75 subvariant are tabulated in Fig. S2. The RBD root-mean-square fluctuation (RMSF) plots of variants and subvariants are plotted in Fig. S3. The RMSF plots mimic the RMSD data, where the delta RBD is most stable. Additionally, the RMSF data indicate that omicron subvariants BA.4/BA.5 and BA2 have stable RBDs.

As mutations serve as markers of genetic variations, it is difficult to quantify their stability; however, mutational effects on the proteins' general stability can be predicted. A recently published article has demonstrated this point, where the S protein mutations within Omicron variant have been found to play roles in allosterically regulating the stability, conformational flexibility and structural adaptability of the protein [26].

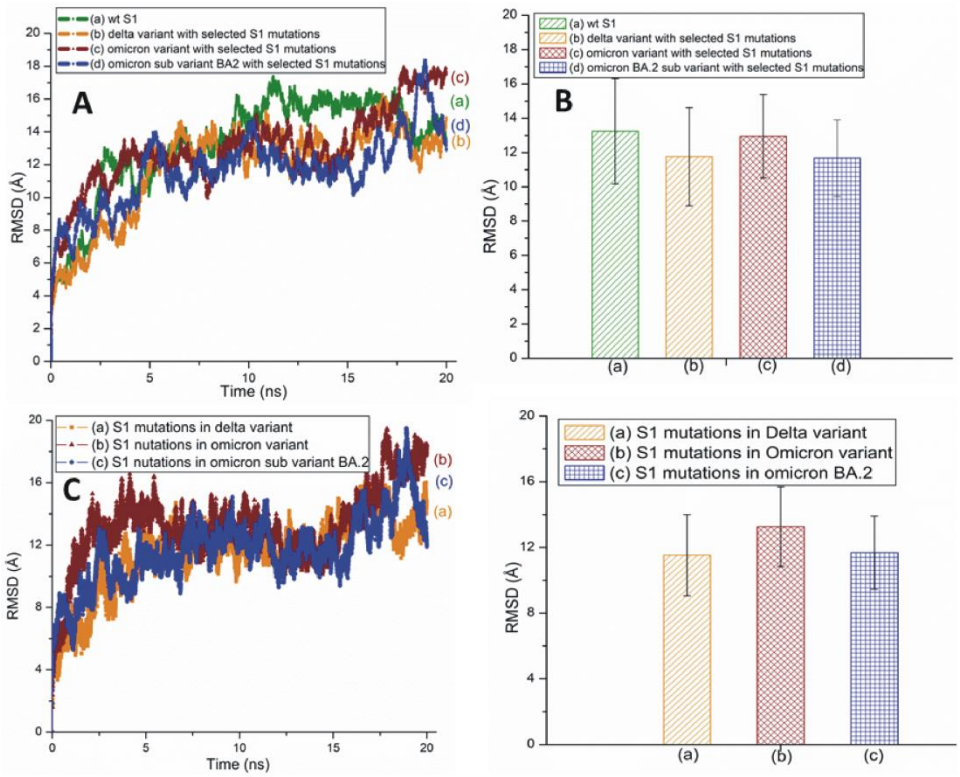

Figure 4. A. The typical all atom RMSD plots of wt and different SARS-CoV-2 variants and subvariant with selected S1 mutations. These variants and subvariant are based on model structure of SARS-CoV-2 S1. B The average RMSD values of wt S1, the Delta and Omicron variants and Omicron subvariant BA.2 with selected S1 mutations. The average RMSD value was taken from a 20ns simulation time. These values were extracted from Fig. 4A. C. The typical RMSD plots of S1 mutations within different SARS-CoV-2 variants and subvariant. D. The average RMSD values of SARS-CoV-2 S1 mutations within deferent variants. The average values were extracted from Fig. 4C.

Fig. 4A represents the traditional all atom RMSD graphs of the wt and the mutant variants of SARS-CoV-2 S1 with selected mutations. Fig 4B shows the average RMSD values of

the wt and variant proteins with selected S1 mutations. From these plots we can infer that the Omicron variant (13.26Å) with S1 mutations show higher RMSD values compare to those of the Delta variant (11.76Å) and BA.2 subvariant (11.67Å). It is also clear from Fig. 4C-D that the S1 mutations within the Delta variant (11.52Å) show the lowest degree of RMSD variations compare to BA.2 (11.68Å) and Omicron (13.26) S1 mutations. Therefore, we can assume that S1 of Delta and BA.2 are the stable form of this virus among these variants and subvariants. The overall all atom RMSD values of the S1 are higher than the RBD RMSDs due to the presence of many turns and coils in this segment. The RMSD plot of Mu S1 is plotted in Fig, S4. From the S1 RMSF plots (Fig. S5) it is clear that Omicron S1 residues have high RMSF values compare to the delta and BA.2 S1. This is particularly prominent in the RBDs of the S1 curated from Figure S5B

Results of time based secondary structure analyses of different RBDs are displayed in Fig. 5. Within the Delta variant, the secondary structure of K417N and L452R mutations are stable compared to T478K (Fig. 5A). In the Omicron variant most of the mutations are unstable including G339D, S371L, S375F, N440K, S477N and T478K, which, in combination, make the Omicron RBD measurably unstable (Fig. 5B). In BA.2 subvariant R408S, T478K and E484A residues seems very stable whereas residues G339D and G496S appear unstable (Fig.5C). These results, suggest an overall high stability of the Delta RBD. Based on its RBD, the subvariant BA.2 is also a stable protein and Omicron RBD is notably unstable among these three RBDs. Most of the mutations identified in BA.4/BA.5, displayed in Fig.5D, are quite stable. Fig. 5E represents the secondary structure changes of the RBD mutations within BA.2.12.1 subvariant. While mutation R408S appears stable with time, according to the present results, mutations

S371F, K417N, T478K and Y505H do not seem to follow the same the same trend. Time based secondary structures of few more variant and subvariants RBDs are displayed in Figs. S6-S8.

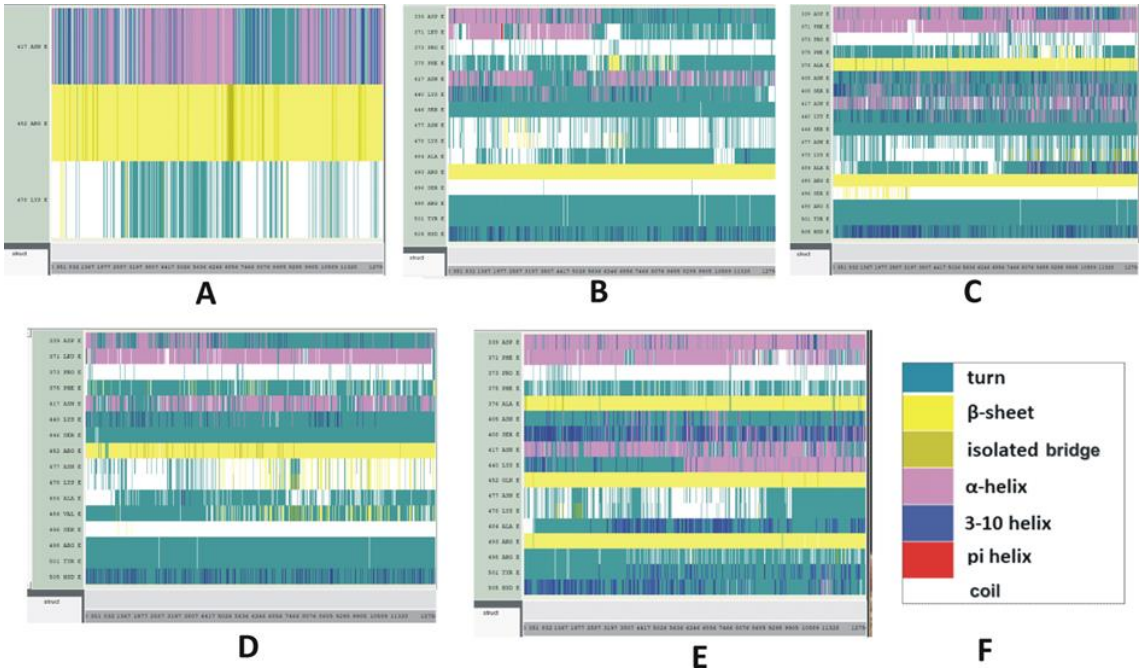

Figure 5. Time based secondary structure changes of SARS-CoV-2 mutant variants and subvariants. The vertical axis represents the mutated residues and the horizontal axis represents the simulation trajectory. A-E. the SARS-CoV-2 RBD of (A) Delta, (B) Omicron variants and Omicron subvariants (C) BA.2 (D) BA.4/BA.5 (E) BA.2.12.1 with selected RBD mutations. These secondary structural changes were recorded for 25ns. F. Color code explanation of proteins' secondary structures. These are the default color codes generated by VMD GUI.

Fig. 6 illustrates the secondary structure changes of SARS-CoV-2 S1 of Delta, and Omicron variants and BA.2 subvariant with selected S1 mutations. The Delta S1 appears quite stable (Fig.6A). No major changes in the stability or fluctuations within the secondary structures are observed for this variant. V70F and T478K residues also seem quite stable during the simulation timescale as the turns and coils of these species are converted into beta sheets. In the case of Omicron S1, though residues G339D and N440K seem stable with time, fluctuations are observed in the mutated residues A67V, L212I, K417N and T547K (Fig. 6B).

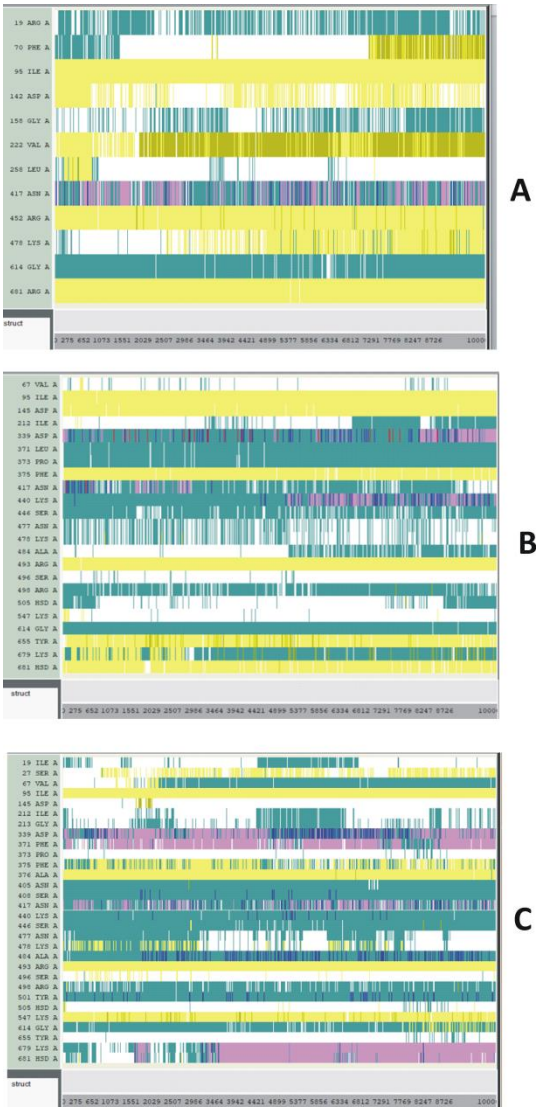

Figure 6. The Secondary structure changes of SARS-CoV-2 S1. A. Delta and B. Omicron variants and C. Omicron subvariant BA.2 with selected S1 mutations. The structural changes were recorded for 20ns.

For the BA.2 subvariant (Fig.6C), residues A67V and T478K seem unstable as their beta sheets are converted into turns and coils. On the other hand, residues S375F and residues 479-81 are converted to alpha helices and beta sheets from their turns/coils phases, respectively. The stability analyses of S1 secondary structure mimics those of the RBD secondary structures, and suggests that Delta is the most stable variant. The secondary structure changes of SARS-CoV-2 S1 within Mu variant is plotted in Fig. S9.

The average solvent accessible surface area (SASA) values for each of the RBD mutations within the SARS-CoV-2 variants and subvariants are plotted in Fig.7. These results

are average SASA values obtained from the simulation time scale. The SASA values are calculated using the VMD timeline window. It should be noted in this context that the severity of certain disease largely depends on the buried or exposed nature of the underlying mutated residues [27]. In Fig. 7A, the highest SASA values are observed in L452R within the RBD of Delta variant, which suggests that this residue has a comparably large solvent accessible surface. The SASA values may increase due to partial unfolding caused by residue mutation.

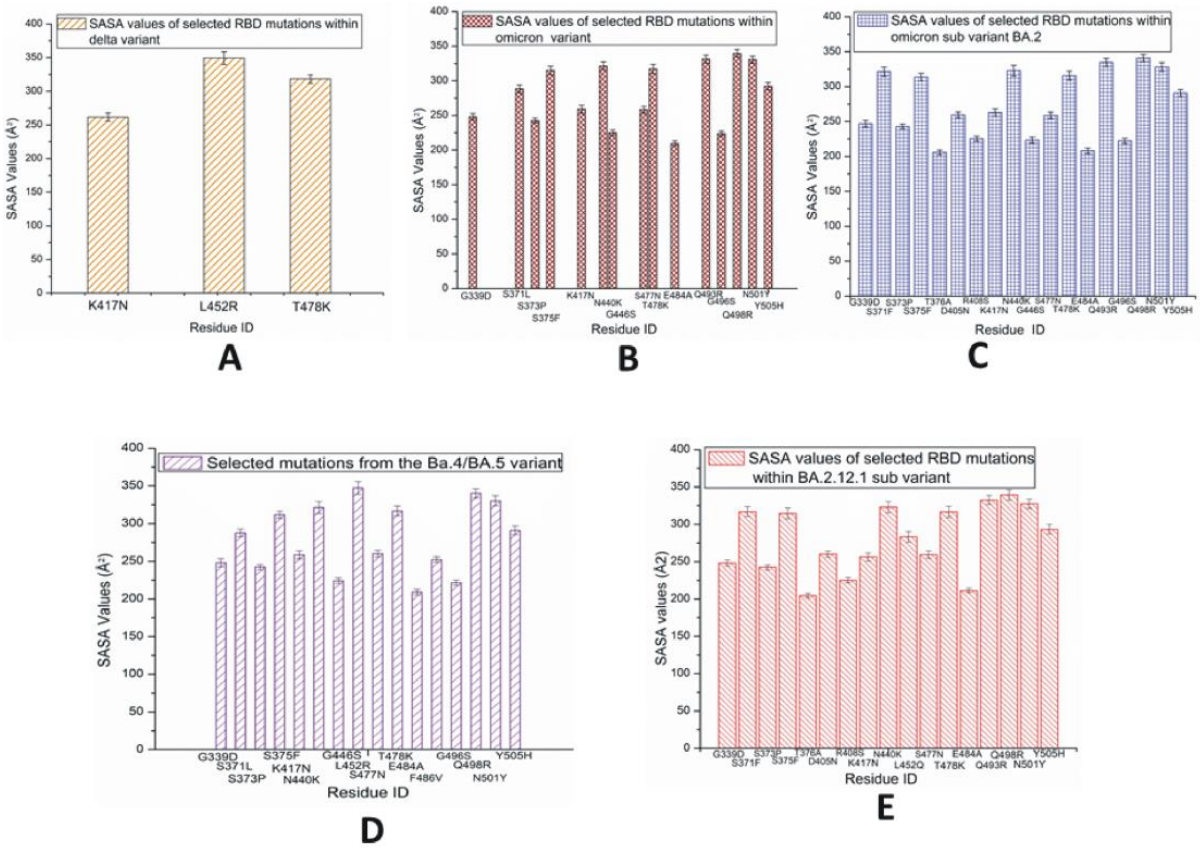

Figure 7. Average SASA values of SARS-CoV-2 RBD mutations observed predominantly in variants A. Delta; B. Omicron and subvariants C. BA.2; D. BA.4/BA.5; and E. BA.2.12.1.

Among the three species we have studied here, the L452R mutation is only observed in the Delta variant. Since mutated residue R is hydrophilic and surface exposed, the structural rearrangements or conformational deviations may possible in this case. Published report suggests that L452R within the Delta variant strongly interacts with ACE2 [28]. T478K within Delta

variant also shows considerably high SASA value. As positively charged K^+ impact the electrostatic surface area, this residue may manifest stronger interactions with the receptor [29]. In Delta RBD, only one residue shows considerably lower SASA values indicating that this buried residue K417N is quite stable in nature. However, if surface exposed residues on the RBD form stable interactions with the ACE2 receptor as in the case of Delta, where the mutant L452R strongly bind to the ACE2 receptor making Delta RBD quite stable. Thus it could be possible that the L452R and T478K within the Delta variant may have a stronger stabilizing effect [14,30]. Although T478K was not present in any previously identified variants, this mutation is observed in all the variants and subvariant we studied in this report. It is possible that the greater mutational fitness of the Delta variant may be due to L452R or a combination of a number of residue mutations.

In the case of Omicron RBD, as displayed in Fig. 7B, despite the presence of fewer buried residues with lower SASA values, majority of the mutated residues have greater SASA values; this suggests the possibility of making this protein quite unstable [31]. The Omicron variant contains more mutations than Delta and some of them are at the ligand-receptor interfacial region, while the stronger binding interactions between L452R and ACE2 receptor make Delta variant somewhat unique. Hydrogen bond formation between residue Q493 of Delta with ACE2 contributes to its stronger structure [28]. Furthermore, it is possible that most of the mutations present in the Omicron variant are counteracted by neutralizing antibodies, while at the same time, L452R in Delta is considered as antibody neutralizing escape mutation. The Omicron and its subvariant BA.4/BA.5 have a lower hydrophobic potential compare to most of the other previously identified variants. Omicron's RBD including the Omicron subvariant BA.4/BA.5 consists of a positive electrostatic surface, while the ACE2 receptor contains many

negatively charged residues; therefore, strong binding due to coulombic interactions at the protein-protein interface region is possible [32]. Moreover, since these positively charged RBD mutations exist within the antibody neutralization epitope regions, they could serve to facilitate immune escape. The charged and hydrophobic surface map of BA.4/BA.5 is displayed in Fig.S10.

In the case of BA.2, as displayed in Fig.7C the slightly higher numbers of buried residues (with lower SASA values) possibly make this subvariant more stable than original Omicron. Usually, the buried residues present within the core of the protein are the most stable part of a protein. The surface exposed residues with greater SASA values are likely to be comparatively less stable unless the surface exposed residues form stronger receptor interactions.

Fig. 7D represents the SASA values of RBD mutations within BA.4/BA.5. Here the additional signature mutation L452R demonstrates higher SASA values compared to the other signature mutation, F486V. As discussed before, L452R plays a key role in receptor residue interaction. Among the other strains studied in this report, mutation L452R is only present in the Delta variant. In BA.2.12.1, the 452 mutation is denoted as L452Q. It is possible that the BA.5 subvariant has become a dominant strain due to the antibody neutralization escape nature of L452R. Considering that the RBDs of BA.4 and BA5 contain mutually similar mutations, certain structural/mutational differences within the S protein may exist that make BA.5 more transmissive than BA.4. Fig. S11 represents the SASA values of a possible subvariant with two mutations L452R and F486V. These two mutations are observed in BA.4/BA.5 in addition to the mutations that are observed in Omicron BA.2.

The SASA values of RBD mutations in BA.2.12.1 are displayed in Fig. 7E. Although some relatively low SASA values are observed, majority of the BA.2.12.1 mutations are surface

exposed and contain greater SASA values. Overall, BA.2 subvariant has more buried residues than those of BA.212.1.

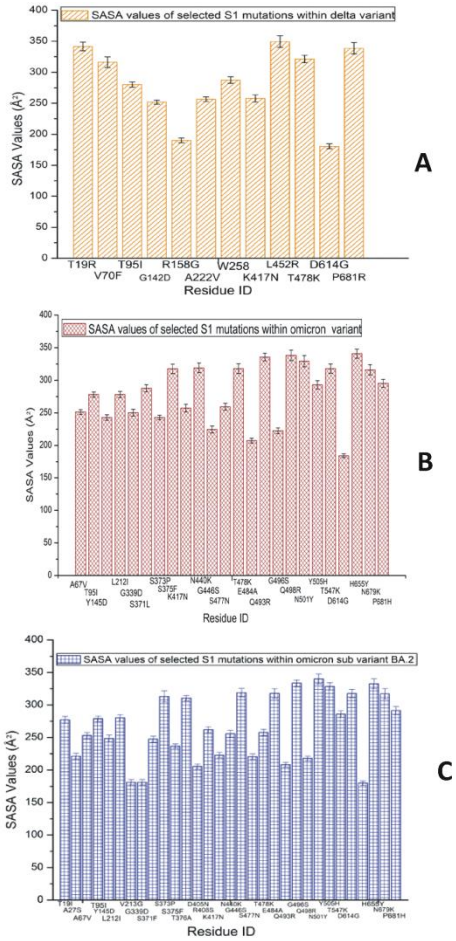

Figure 8. Average SASA values of SARS-CoV-2 S1 mutations observed predominantly in A. Delta variant; B. Omicron variant; and C. Omicron subvariant BA.2.

The SASA values of S1 mutations are displayed in Fig 8A-C, where the findings of the corresponding RBDs are detected again. The Delta has a number of buried residues, but here the surface exposed residues have strong interactions with ACE2. Despite the many buried residues of Omicron, the numbers of surface exposed residues are greater than the buried residues in this case. S1 of subvariant BA.2 has more buried residues than those of the S1 of Omicron variant. It is likely that most of the surface exposed residues in the Omicron variant are loosely attached to the ACE2 receptor. Currently there are no readily available experimental results for the BA.2 subvariant. This subvariant may have antibody neutralizing escape mutants and thus, may

emerge as a strong form of the virus [33,34]. Nonetheless, according to the RMSD data and the time-based secondary structure analyses of S1 data presented here, the Delta and subvariant BA.2 are the stable forms among the three forms we have studied. For the RBD structure, BA.4/BA.5 is also quiet stable along with the them. Since most of the mutations in BA.4, BA.5 and BA2.12.1 are concentrated and hence observed in their RBDs, we have specifically examined the RBDs of these three subvariants in the present report.

Omicron subvariant BA.2 has been known as "stealth Omicron" as this subvariant was initially difficult to identify from the Delta variant using traditional testing procedures. A combination of subvariants BA.1 and BA.2 has been also identified. This hybrid or recombinant variant is also known as subvariant XE [35]. Very recently, a BA.5 sublineage BF.7, has been reported, that contains S1 RBD mutation R346T in addition to the BA.5 mutations [36,37]. Based on the limited information currently available it could be predicted that BF.7 has higher spreadibility with short incubation time and greater antibody neutralization escape efficacy [38].Glycosylation sites are important as they play critical roles in immune evasion. Since BF.7 has mutation R346T close to N331 and N343 (two N-linked glycosylation sites of S1 RBD), that could possibly be linked to higher immune escape [32,39].

4. Conclusions

The simulation data reported here indicate that Delta is a stable form of COVID 19. However, among the forms selected for the present study, BA.4/BA.5 and BA.2 RBD also appears very stable. Additionally, some of the mutations discussed in this report play crucial role in formation of stable variants/subvariants. Recently the mRNA bivalent boosters have been released in US that contain mRNA of original wt strain as well as BA.4/BA.5 subvariants and

thus are more effective against aggressive infections. However as mRNA virus is highly adaptable and environmentally fit, it is possible that newer versions of variants/subvariants with new functional epitopes may emerge with possible breakthrough infections. We expect that the detailed structural data discussed in this paper will be useful to identify drug targets and neutralizing antibodies for emerging SARS-CoV-2 variants or subvariants. We also hope that by contributing to the literature on SARS-CoV-2, the present manuscript will serve to help the ongoing efforts to overcome the COVID 19 pandemic in some ways.

Supplementary Materials

Figs S1-S11; Table S1-SII

Conflict of interest statement

The author declares no conflict of interest.

Acknowledgments

The author acknowledges utilization of the following simulation and visualization software packages: 1) NAMD and 2) VMD: NAMD and VMD, developed by the Theoretical and Computational Biophysics Group in the Beckman Institute for Advanced Science and Technology at the University of Illinois, Urbana-Champaign. 3) Discovery Studio Visualizer: Dassault Systèmes BIOVIA, Discovery Studio Modeling Environment, San Diego, CA: Dassault Systèmes (2015).

References

1. WHO, Weekly epidemiological update (2021). Available online: https://www.who.int/publications/m/item/weekly-epidemiological-update---23-february-2021 (accessed on 25 February 2021).
2. https://www.cdc.gov/coronavirus/2019-ncov/variants/variant-info.html#Interest. Centers for Disease Control and Prevention, SARS-CoV-2 Variant Classifications and Definitions. Available online: https://www.cdc.gov/coronavirus/2019-ncov/variants/variant-info.html#Interest. (accessed on June 22, 2021, July 26, 2021, December7, 2021, April 26, 2022, June, 2022).
3. https://www.cdc.gov/coronavirus/2019-ncov/science/science-briefs/scientific-brief-omicron-variant.html. Science Brief: Omicron (B.1.1.529) Variant. Available online: https://www.cdc.gov/coronavirus/2019-ncov/science/science-briefs/scientific-brief-omicron-variant.html (accessed on February 18, 2022).
4. https://covariants.org/variants/21L.Omicron. Variant: 21L (Omicron) also known as BA.2. Available online: https://covariants.org/variants/21L.Omicron (accessed on March 22, 2022).
5. SARS-CoV-2 variants of concern as of 9 June 2022. Available online: https://www.ecdc.europa.eu/en/covid-19/variants-concern (accessed on June 17, 2022, July 12, 2022).
6. Tracking SARS-CoV-2 variants. Available online: https://www.who.int/en/activities/tracking-SARS-CoV-2-variants/ (accessed on June 14, 2022).
7. Lampe, A.T.; Puniya, B.L.; Pannier, A.K.; Helikar, T.; Brown, D.M. Combined TLR4 and TLR9 agonists induce distinct phenotypic changes in innate immunity in vitro and in vivo. *Cell. Immunol.* **2020**, *355*, 104149.
8. Haspel, N.; Jang, H.; Nussinov, R. Active and Inactive Cdc42 Differ in Their Insert Region Conformational Dynamics. *Biophys. J.* **2021**, *120*, 306-318.
9. Schneidman-Duhovny, D.; Wolfson, H.J. Modeling of Multimolecular Complexes. *Methods Mol. Biol.* **2020**, *2112*, 163-174.
10. Roy, U. Structural Characterizations of the Fas Receptor and the Fas-Associated Protein with Death Domain Interactions. *The Protein J.* **2016**, *35*, 51-60.
11. Roy, U. 3D Modeling of Tumor Necrosis Factor Receptor and Tumor Necrosis Factor-bound Receptor Systems. *Mol. Inform.* **2019**, *38*, e1800011.
12. Roy, U. Structural and molecular analyses of functional epitopes and escape mutants in Japanese encephalitis virus envelope protein domain III. *Immunol. Res.* **2020**, *68*, 81-89.
13. Roy, U. Role of N501Y mutation in SARS-CoV-2 spike proteinstructure. *Preprints, 2021060238* **2021**.
14. Roy, U. Comparative Structural Analyses of Selected Spike Protein-RBD Mutations in SARS-CoV-2 Lineages. *Immunol. Res.* **2021**, *70*, 143-151.
15. Fatouros, P.R.; Roy, U.; Sur, S. Modeling Substrate Coordination to Zn-Bound Angiotensin Converting Enzyme 2. *Int. J. Pept. Res. Ther.* **2022**, *28*, 65.
16. Tanner, D.E.; Phillips, J.C.; Schulten, K. GPU/CPU Algorithm for Generalized Born/Solvent-Accessible Surface Area Implicit Solvent Calculations. *J. Chem. Theory Comput.* **2012**, *8*, 2521-2530.
17. Wang, Q.; Guo, Y.; Iketani, S.; Nair, M.S.; Li, Z.; Mohri, H.; Wang, M.; Yu, J.; Bowen, A.D.; Chang, J.Y.; et al. Antibody evasion by SARS-CoV-2 Omicron subvariants BA.2.12.1, BA.4 and BA.5. *Nature* **2022**, *608*, 603-608.
18. Lan, J.; Ge, J.; Yu, J.; Shan, S.; Zhou, H.; Fan, S.; Zhang, Q.; Shi, X.; Wang, Q.; Zhang, L.; et al. Structure of the SARS-CoV-2 spike receptor-binding domain bound to the ACE2 receptor. *Nature* **2020**, *581*, 215-220.

19. Yang, J.; Zhang, Y. I-TASSER server: new development for protein structure and function predictions. *Nucleic Acids Res.* **2015**, *43*, W174-181.
20. Walls, A.C.; Park, Y.J.; Tortorici, M.A.; Wall, A.; McGuire, A.T.; Veesler, D. Structure, Function, and Antigenicity of the SARS-CoV-2 Spike Glycoprotein. *Cell* **2020**, *181*, 281-292.e286.
21. Xiong, X.; Qu, K.; Ciazynska, K.A.; Hosmillo, M.; Carter, A.P.; Ebrahimi, S.; Ke, Z.; Scheres, S.H.W.; Bergamaschi, L.; Grice, G.L.; et al. A thermostable, closed SARS-CoV-2 spike protein trimer. *Nat. Struct. Mol. Biol.* **2020**, *27*, 934-941.
22. Humphrey, W.; Dalke, A.; Schulten, K. VMD: Visual molecular dynamics. *J. Mol. Graph.* **1996**, *14*, 33-38.
23. Phillips, J.C.; Braun, R.; Wang, W.; Gumbart, J.; Tajkhorshid, E.; Villa, E.; Chipot, C.; Skeel, R.D.; Kale, L.; Schulten, K. Scalable molecular dynamics with NAMD. *J. Comput. Chem* **2005**, *26*, 1781-1802.
24. Ribeiro, J.V.; Bernardi, R.C.; Rudack, T.; Stone, J.E.; Phillips, J.C.; Freddolino, P.L.; Schulten, K. QwikMD - Integrative Molecular Dynamics Toolkit for Novices and Experts. *Sci. Rep.* **2016**, *6*, 26536.
25. Dassault Systèmes BIOVIA *Discovery Studio Modeling Environment, San Diego, CA: Dassault Systèmes (2015).*
26. Verkhivker, G.M.; Agajanian, S.; Kassab, R.; Krishnan, K. Frustration-driven allosteric regulation and signal transmission in the SARS-CoV-2 spike omicron trimer structures: a crosstalk of the omicron mutation sites allosterically regulates tradeoffs of protein stability and conformational adaptability. *Physical Chemistry Chemical Physics* **2022**, *24*, 17723-17743.
27. Savojardo, C.; Manfredi, M.; Martelli, P.L.; Casadio, R. Solvent Accessibility of Residues Undergoing Pathogenic Variations in Humans: From Protein Structures to Protein Sequences. *Front Mol. Biosci.* **2020**, *7*, 626363.
28. Socher, E.; Heger, L.; Paulsen, F.; Zunke, F.; Arnold, P. Molecular dynamics simulations of the delta and omicron SARS-CoV-2 spike - ACE2 complexes reveal distinct changes between both variants. *Comput. Struct. Biotechnol. J.* **2022**, *20*, 1168-1176.
29. Di Giacomo, S.; Mercatelli, D.; Rakhimov, A.; Giorgi, F.M. Preliminary report on severe acute respiratory syndrome coronavirus 2 (SARS-CoV-2) Spike mutation T478K. *J. Med. Virol.* **2021**, *93*, 5638-5643.
30. Goher, S.S.; Ali, F.; Amin, M. The Delta Variant Mutations in the Receptor Binding Domain of SARS-CoV-2 Show Enhanced Electrostatic Interactions with the ACE2. *Med. Drug Discov.* **2021**, 100114.
31. Zeng, C.; Evans, J.P.; Qu, P.; Faraone, J.; Zheng, Y.-M.; Carlin, C.; Bednash, J.S.; Zhou, T.; Lozanski, G.; Mallampalli, R.; et al. Neutralization and Stability of SARS-CoV-2 Omicron Variant. *bioRxiv* **2021**, 2021.2012.2016.472934.
32. López-Cortés, G.I.; Palacios-Pérez, M.; Veledíaz, H.F.; Hernández-Aguilar, M.; López-Hernández, G.R.; Zamudio, G.S.; José, M.V. The Spike Protein of SARS-CoV-2 Is Adapting Because of Selective Pressures. *Vaccines (Basel)* **2022**, *10*.
33. Chen, J.; Wei, G.-W. Omicron BA.2 (B.1.1.529.2): high potential to becoming the next dominating variant. *ArXiv* **2022**, arXiv:2202.05031v05031.
34. Kannan, S.R.; Spratt, A.N.; Sharma, K.; Sönnerborg, A.; Apparsundaram, S.; Lorson, C.; Byrareddy, S.N.; Singh, K. Complex Mutation Pattern of Omicron BA. 2: Evading Antibodies without Losing Receptor Interactions. *Int. J. Mol. Sci.* **2022**, *23*, 5534.
35. https://www.foxnews.com/health/covid-19-subvariant-xe-ba-2-coronavirus-pandemic. COVID-19 subvariant XE: What to know. Available online: https://www.foxnews.com/health/covid-19-subvariant-xe-ba-2-coronavirus-pandemic (accessed on accessed May 10, 2022).

36. WHO, Tracking SARS-CoV-2 variants. Available online: https://www.who.int/activities/tracking-SARS-CoV-2-variants (accessed on 22 December, 2022).
37. SARS-CoV-2 variants of concern and variants under investigation in England, Technical briefing 46. Available online: https://assets.publishing.service.gov.uk/government/uploads/system/uploads/attachment_data/file/1115070/Technical-Briefing-46-7October2022.pdf (accessed on 22 December, 2022).
38. BF.7: What to know about the Omicron COVID variant. Available online: https://www.cbsnews.com/news/bf7-new-omicron-coronavirus-variant-covid/ (accessed on 22 December 2022).
39. Watanabe, Y.; Allen, J.D.; Wrapp, D.; McLellan, J.S.; Crispin, M. Site-specific glycan analysis of the SARS-CoV-2 spike. *Science* **2020**, *369*, 330-333.